THE EFFECT OF SUBSTRATE TEMPERATURE AND ANNEALING ON THE PHOTORESPONSE OF ZnO UV SENSOR

HALIM BIN AHMAD

UNIVERSITI SAINS MALAYSIA

2013

THE EFFECT OF SUBSTRATE TEMPERATURE AND ANNEALING ON THE PHOTORESPONSE OF ZnO UV SENSOR

by

HALIM BIN AHMAD

Thesis submitted in fulfillment of the requirements

for the Degree of

Master of Science

December 2013

ACKNOWLEDGEMENT

I would love to first and foremost give all the glory to Allah SWT the Most Merciful the Most Compassionate. For Allah SWT has shown me the light throughout my life and throughout this research that have made everything hard became ease and possible. Even when looking back, I know that I did not and could not have done this research in my own strength.

My academic advisor, Professor Mat Johar Abdullah, deserves my sincerest gratitude for providing me the opportunity to conduct this research. The knowledge, guidance and patience he so kindly offered to me at every stage of the project has been crucial for the success of my exploration of the semiconductor's world of physics.

This work would not have been possible without the help and contribution of many individuals. I wish to extend my heartfelt thanks to all my faculty member, office staff and technical staff of Nano Optoelectronics Research Lab especially to En. Mohktar, En. Jamil and En. Hazhar for their limitless cooperation. I also wish to express my great appreciation to my friend Mohammad Rasheed, Ooi Poh Kok and Marzaini for their irreplaceable encouragement, good humor and partnership whom without them the journey of this research would be very dull. I am indebted to my senior Naif Al Hardan whom I have learned a lot from and if not because of him I would have not finished my work.

No words would ever do justice to express my deepest thanks and gratitude to my lovely wife Dg. Haryani Diana through continuous love, patience, sacrifice, invaluable support and constant encouragement have allowed me to pursue my ambitions. It is to her I dedicate this thesis.

TABLE OF CONTENTS

LIST OF TABLES

LIST OF FIGURES

LIST OF PLATES

Page

LIST OF ABBREVIATIONS

ZnO	Zinc Oxide
SiO_2	Silicone dioxide
GaN	Gallium Nitride
UV	Ultraviolet
I-V	Current-Voltage
Ar	Argon
PL	Photoluminscence
AFM	Atomic Force Microscopy
XRD	X-ray diffraction
SEM	Scanning electron microscopy
FESEM	Field effect Scanning electron microscopy
EDX	Energy dispersive X-ray
Wz	Wurtzite
UPS	Ultraviolet photoelectron spectroscopy
NEP	Noise Equivalent Power

LIST OF SYMBOLS

κ	thermal conductivity
E	bulkYoung modulus
H	bulk hardness
D^+	detectivity
Bw	bandwidth
R	responsivity
η	quantum efficiency
t_r	rising time
t_d	decay time
r	resistivity
n	free electron concentration
e	fundamental electronic charge
μ_H	Hall mobility
r_H	Hall scattering factor
λ	wavelenght
g	gain
h	Planck's constant
c	speed of light

KESAN SUHU SUBSTRAT DAN PENYEPUHLINDAPAN KE ATAS TINDAKBALAS CAHAYA PENDERIA UV BERASASKAN ZNO

ABSTRAK

Zink Oksida (ZnO) adalah Semikonduktor sebatian kumpulan II-VI yang memiliki jurang jalur langsung 3.37 eV dan tenaga ikatan eksiton tinggi sebanyak 60 MeV. Justeru itu, peranti optoelektronik berasaskan ZnO yang berfungsi di dalam julat UV telah dikaji secara meluas. ZnO dikatakan mempunyai potensi dalam aplikasi yang pelbagai, oleh itu banyak percubaan untuk menghasilkan struktur nano ZnO telah berjaya dihasilkan. Dalam kajian ini, satu kerja telah dijalankan untuk menyintesis, mempercirikan dan memfabrikasi peranti penderia cahaya UV berasaskan ZnO. Semua struktur nano ZnO disintesis dengan memendapkan ZnO pada substrat SiO_2/Si. Hasil dari kajian ini telah dibahagikan kepada tiga bahagian. Bahagian pertama adalah untuk menentukan ciri-ciri sampel ZnO yang telah dimendapkan pada suhu substrat yang berbeza dan kemudian menjalani rawatan haba pada 900 ° C. Penemuan bahagian ini termasuk peningkatan kualiti kristal dan optik kerana rawatan haba- dengan meningkatkan suhu pemendapan (Suhu Bilik 200°C dalam eksperimen ini) menyediakan atom-atom dengan tenaga pengaktifan yang cukup untuk meresap ke dalam kawasan atom yang stabil dalam kekisi kristal dan membenarkan bendasing untuk berpindah ke sempadan bijian, menyebabkan pembentukan kristal-kristal besar melalui kelompok pengasaran, demonstrasi pelepasan cahaya UV dan hijau menunjukkan intensitinya adalah bergantung kepada suhu. Penurunan ketara dalam pereputan masa t_d juga berjaya dikesan. Bahagian kedua adalah untuk menentukan ciri-ciri sampel ZnO yang dimendapkan kepada ketebalan filem yang berbeza. Penemuan bahagian ini termasuk peningkatan dalam intensiti PL dengan bertambahnya ketebalan filem. Nisbah arus electrik cahaya UV kepada arus elektrik cahaya gelap yang paling maksima adalah pada

ketebalan 1230 nm. Manakala sampel ini turut mencatatkan masa kenaikan terpantas sebanyak 128.5 s. Bahagian terakhir adalah untuk menentukan ciri-ciri optoelektrik pada peranti penderia cahaya UV yang mempunya reka bentuk yang berbeza, termasuk penderia cahaya UV Schottky berganda dan MSM. Telah dibuktikan bahawa penyerapan oksigen dan nyahpenyerapan berasal sama ada dari proses keadaan pejal atau yang berkaitan dengan permukaan memainkan peranan penting dalam mengawal reaksi cahaya [155].Didapati bahawa ketinggian halangan Schottky di antara muka (Ag/ZnO) pada sampel yang disediakan dan dirawat haba adalah masing-masing sekitar 0.74 dan 0.76 eV. Kebocoran arus elektrik yang lebih baik bagi sampel yang telah dirawat haba dan pereputan masa yang lebih cepat untuk peranti Al/ZnO/Ag juga telah berjaya ditunjukkan.

THE EFFECT OF SUBSTRATE TEMPERATURE AND ANNEALING ON THE PHOTORESPONSE OF ZnO UV SENSOR

ABSTRACT

Zinc Oxide (ZnO) is a II-VI compound semiconductor with a direct band gap of 3.37 eV and a high exciton binding energy of 60 meV. Thus, ZnO based optoelectronic devices working in UV region have been studied extensively. For the wide applications of ZnO, numerous ZnO thin films nanostructure preparations have been successfully attempted. In this work, a coherent effort has been carried out on the synthesis, characterization and device fabrication of ZnO based UV photodetector. All ZnO nanostructures were synthesized by depositing ZnO on SiO_2/Si substrates. The results of this work have been divided into three parts. The first part was to characterize the ZnO sample that was deposited at different substrate temperatures and then undergone heat treatment at 900 °C. The findings of this part include improvement of the crystalline and optical quality due to heat treatment-by increasing the deposition temperature (Room Temperature to 200 °C in this experiment) provides atoms with enough activation energy to diffuse into the stable atomic sites in the crystal lattice and impurities to move to grain boundary, resulting in forming large crystallites through cluster coarsening, the demonstration of UV and green emissions showing its intensity was temperature dependence. Significant drop in decay time t_d in photoresponse was also revealed. The second part was to characterize the ZnO sample deposited to different thickness. The findings of this part include the rise in PL intensity as the thickness increase. The maximum UV illuminated current to leakage current was at the thickness of 1230 nm. This sample also recorded the fastest rise time of 128.5 s. The last part was to characterize the optoelectrical properties of different design of UV Photodetector, which include the double Schottky barrier and MSM UV photodetectors. It has been observed that oxygen adsorption and desorption originating either from a solid state or surface related process

plays an essential part in control of the photoresponse [155]. It was also found that the Schottky barrier heights for the as prepared and heat treated Ag/ZnO interface was around 0.74 and 0.76 eV respectively. Improved leakage current for the heat treated sample and faster decay time for the Al/ZnO/Ag device were exhibited.

CHAPTER 1-INTRODUCTION

1.1. Background of Study- Wide Band Gap Semiconductor

As the name point out, a “wide bandgap” semiconductor is define as having a large bandgap energy, which is directly associated to the emission/absorption wavelength of optical devices. Wide bandgap semiconductors usually exhibit emission/absorption wavelengths in the green/blue part of the visible spectrum and in the shorter wavelengths of violet/ultraviolet light. As an example, a well-known application of wide bandgap semiconductors is the “blue light emitting diode”. Hence in general, wide bandgap semiconductors can be defined as having fundamental optical absorption boundaries that are of shorter wavelengths than the color red. Semiconductor light emitting devices are high efficiency, light weight, miniature in size, and possess much longer lifetimes than other light sources. Specifically, wide bandgap semiconductors have become increasingly important in the electronics industry as optical sources for full color displays, UV/deep UV light sources, white light illumination and blue–violet laser diodes for high density DVDs. However in spite of the great world-wide interest in the use of wide bandgap semiconductors for blue LEDs, a long time passed before technological breakthroughs led to the fabrication of p-n junctions in GaN. After 1990, the number of researchers involved in wide bandgap semiconductors increased dramatically following the first successful operation of the blue LED [1]. The three main types of wide bandgap semiconductors are:

a) Group III nitrides such as GaN

b) Group II oxides such as ZnO

c) Group II chalcogenides such as ZnSe

1.1.1. ZnO

Zinc oxide (ZnO), is a wide-band-gap semiconductor (*Eg* = 3.37 eV at room temperature) with a large exciton binding energy of 60meV that is suitable for short wavelength optoelectronic applications. Nanostructured ZnO materials have received broad attention due to their distinguished performance in electronics, optics and photonics. ZnO is also a key technological material. The morphology of ZnO has been proven to be the richest among inorganic semiconductors. Up to now, ZnO nanoarrays, nanorods, nanowires, nanobelts, nanotubes, nanorings, nanohelices, and nanosprings have been synthesized via a variety of techniques, such as template-assisted growth, vapor-liquid-solid methods, chemical vapour deposition, and solution-based synthesis [12–21].

1.1.2. UV Photodetector

Ultraviolet (UV) detectors exploiting transparency in the visible region are examples of wide bandgap semiconductor photodetectors. Such solar blind UV detectors that are insensitive to visible light and respond only to UV irradiation are used as flame sensors and to detect harmful UV radiation in sunlight [22]. High efficiency, photovoltaic type detectors have been fabricated and their simple structure has led to interest in photoconductive types of detectors as well [45-49].

1.1.3. ZnO as a UV Photodetector

The growth and material characteristics of semiconductor with wide band gaps have been studied with a great extend of scope aiming at developing electronic devices based on III-Nitrides semiconductor (GaN), II-Oxides (ZnO), II Chalcogenides (ZnSe) and other based of semiconductor such as GaAs, TiO2, GeO2 and SiC. Of these entire compounds, ZnO is among the most attractive and extensively studied wide band gap material. Owing to its unique properties such as non-toxicity, abundant in nature, large band gap (3.37ev), high melting temperature, higher exciton binding energy at 60 meV, than those of other

semiconductors such as GaAs (5mev), ZnSe (19mev) GaN (24meV) and 3C-SiC (17 mev). Based on these distinctive characteristic, ZnO has been extensively studied in numerous applications, including transistors [23-25], pyroelectric devices [26-27], piezoelectric devices [28-30], surface acoustic devices [31-32], gas sensors and solar cells[33-38]. ZnO as a II-VI semiconductor compound has recently become an attractive material due to its applications potential for optoelectronic devices such as light emitting device (LED) operating in the blue/ultraviolet (UV) region of the spectrum [39-42], laser diodes (LDs) [43-44] and lately UV photodetectors [45-61]. Recently UV photodetectors are becoming significant in number of areas such as UV astronomy, radiation dosimetry, reagent detectors, missile warning systems and etc. [43-44]. Metal-Semiconductor-Metal (MSM) structures such as Schottky diodes and simple photoconductive devices are regularly applied as photodetectors. Schottky diodes have some advantages over photoconductive devices such as the simplicity of fabrication, compatibility with field effect transistors and their improving performance. The reports of ZnO UV photodetector mainly focus on MSM structures which contains Ohmic contacts based photoconductive type [45-49] and Schottky barrier based photovoltage type [50-53].UV light detection with ZnO has created a lot of interest for selective photodetector applications (365 nm) [47, 54-55]. The increasing interest in the sensor field has led many researchers to investigate the possibility of widening the band gap of ZnO by alloying with Cd and Mg to extend over UV-A, UV-B and UV-C region [62-65]. Over the last several years, various techniques have been used to deposit *c*-axis oriented ZnO films including molecular beam epitaxy (MBE) [66], metal organic chemical vapor deposition (MOCVD) [67], atomic layer deposition (ALD)[68], sol-gel technique [69], spray pyrolisis [70], pulse laser deposition(PLD)[71], photo-enhanced chemical vapor deposition (P-E CVD)[72], and radio frequency (R.F) sputtering [73]. RF sputtering is by far the most common technique used to deposit ZnO films. The advantages of RF sputtering compared with other deposition techniques are dense layer formation, high deposition rate, low growth temperature, low cost and so on.

1.2. Problem Statement

The optimization of ZnO thin films has been an important step towards realizing high quality micro devices. Insufficient knowledge regarding the effect of substrate temperature and annealing of ZnO thin film towards the behaviour of ZnO UV detecting devices has propelled and initiated this study. Several studies have also shown the advantage of MSM structure for fabricating ZnO UV photodetector [65] but the data regarding these type of structure is still lacking. It can be assumed that there is a need to investigate MSM structure in order to enhance the performance of it UV detecting properties.

1.3. Objectives of Study

This research concentrated on nanostructured ZnO thin film produced by RF sputtering. SiO_2/Si was used as substrates. Main concern is on the ZnO synthesis condition and post annealing effect. The properties of the grown ZnO such as surface morphologies, optical, electrical and photoresponse were the core study of this work.

The objectives of the work are:

1. To grow ZnO thin films via RF sputtering technique. Variations in the growth parameters such as substrates temperature, film thickness and gas partial pressures are to be explored and trying to find its significance towards the morphological alterations of the ZnO nanostructures. The synthesized ZnO microstructures morphological growth will be studied by microscopic and spectroscopic analyses such as X-ray diffraction (XRD), field emission scanning electron microscopy, atomic force microscopy (AFM) and energy dispersive X-ray(EDX).
2. To study the intrinsic defects of the ZnO nanostructures via photoluminescence (PL).
3. To fabricate two designs of UV photodetector based on ZnO thin film. Current-voltage (IV) is to be characterized for leakage and UV-photoilluminated current.

The performance of the photodetector will be measured by its time response properties.

1.4. Scopes of Study

ZnO is a widely researched semiconducting material and was intensely investigated over the last few decades. A reasonable range of study is made as to set an appropriate target for this thesis. Merely results and discoveries that are corresponding to the scope as denoted here are to be comprised in the thesis.

a) Crystallography and Surface structure of ZnO

This work investigates mainly on the ZnO growth by RF sputtering technique and some analyses were made via X-ray diffraction, Field-emission scanning electron microscope and Atomic force microscopy.

b) Fabrication of a simple UV photodetector based on ZnO

The fabricated UV photodetector was designed in the form of MSM structure.

c) ZnO thin film and UV Photodetector Optoelectronic Characterization

Optical characterization of ZnO thin film was carried out by photoluminescence spectroscopy, from which the intrinsic defect of the ZnO can be correlated to the behaviour of the fabricated UV photodetector. IV and time dependent photoresponse measurement was also done to the UV photodetector as a performance indicator.

1.5. Organization of Thesis

The main goal of this dissertation is to fabricate UV photodetector based on ZnO nanostructure thin film prepared through RF magnetron sputtering.

Chapter 2 introduces relevant literature survey of this study which contains important theory of ZnO and UV detecting devices.

Chapter 3 explains comprehensive description of the experimental set up and execution. In this chapter, we show the method of ZnO growth and how it is characterised by using some experimental equipment that we have in our laboratory and some were from outside. We have also shown how the UV photodetector were fabricated and tested.

Chapter 4 is where the results of the experiment were compiled. The data collected were visualized into suitable method (graph, table, etc.) as to make the results more distinct, comprehensible and easier to describe. The results of the ZnO thin film morphologies, structures and PL properties were also discussed in this chapter.

Chapter 5 mainly discuss and analyse the electrical properties and performance of the ZnO UV photodetector. Relevant current investigation and research were inferred towards the outcome of this study.

Chapter 6 reiterates the findings of this study and proposed some recommendations for future research based on the outcomes that may improve or expand the knowledge of this study.

CHAPTER 2-LITERATURE REVIEW

2.1. ZnO For Several Applications

ZnO has been drawing considerable attention from material researchers in recent times. In the past several decades, dating back as early as 1932 it has featured as a topic of interest of thousands of research papers [74-76]. Greatly appreciated for its high energy (ultra violet) absorbance, piezoelectricity, wide chemical properties and luminescence at high operating temperatures, ZnO has been used far into industry, and is one of the significant forming materials in today's modern society [77-78]. To name just a few, it can be found in paints, electronics, rubber and plastics industries, cosmetics and pharmaceutical manufacturing. Yet more recently, ZnO has once more re-appeared in the scientific society attention, this time for its exceptional semiconducting properties [79]. Driven up by the improvement in growth technologies and the prospective for ZnO to become a fitting alternative for the expensive GaN, the fabrication of highly *c*-axis oriented ZnO [72-73,80-83], high quality single crystal and epitaxial layers was succeeded [83-87]. Making way for the realization of ZnO based photonic and optoelectronic devices, whereas, amongst other potential applications it stands with GaN as a future candidate for the next generation of light emitters and laser diodes for solid state lighting applications [86-88]. With a wide band gap of 3.37 eV and a large exciton binding energy of 60 meV at room temperature, ZnO offers extraordinary promise for blue and ultraviolet optical devices. Even though GaN and GaN-based semiconductors have dominated and widely studied in this wavelength range, ZnO enters the field with some unique benefits [89].

2.2. General properties of ZnO

In this chapter, an overview of the basic properties of ZnO, including the crystal structure, energy band structure and thermal properties is presented, as well as an introduction to the mechanical properties, basic electronic and optical properties and potential applications of ZnO.

2.2.1. Crystal structure and lattice parameters

Generally most of the group II–VI binary compound semiconductors crystallize in either cubic zinc blende or hexagonal wurtzite (Wz) structure where each anion is surrounded by four cations at the corners of a tetrahedron, and vice versa. At ambient pressure and temperature, ZnO crystallizes in the wurtzite (B4 type) structure, as shown in figure 2.1 (a). This is a hexagonal lattice, belonging to the space group $P6_3mc$, and is characterized by two interconnecting sublattices of Zn^{2+} and O^{2-}, such that each Zn ion is surrounded by a tetrahedra of O ions, and vice-versa. This tetrahedral coordination gives rise to polar symmetry along the hexagonal axis. This polarity is responsible for a number of the properties of ZnO, including its piezoelectricity and spontaneous polarization, and is also a key factor in crystal growth, etching and defect generation. The four most common face terminations of wurtzite ZnO are the polar Zn terminated (0001) and O terminated $(000\bar{1})$ faces (*c*-axis oriented), and the non-polar $(11\bar{2}0)$ (*a*-axis) and $(10\bar{1}0)$ faces which both contain an equal number of Zn and O atoms. The polar faces are known to posses different chemical and physical properties, and the O-terminated face possess a slightly different electronic structure to the other three faces [90]. Additionally, the polar surfaces and the (1010) surface are found to be stable, however the $(11\bar{2}0)$ face is less stable and generally has a higher level of surface roughness than its counterparts. The (0001) plane is also basal. Aside from causing the inherent polarity in the ZnO crystal, the tetrahedral coordination of this compound is also a common indicator of sp^3 covalent bonding.

However, the Zn–O bond also possesses very strong ionic character, and thus ZnO lies on the borderline between being classed as a covalent and ionic compound, with an ionicity of f_i =0.616 on the Phillips ionicity scale [91]. The lattice parameters of the hexagonal unit cell are a=3.2495Å and c=5.2069 Å, and the density is 5.605 g cm^{-3} [92]. In an ideal wurtzite crystal, the axial ratio c/a and the u parameter (which is a measure of the amount by which each atom is displaced with respect to the next along the c-axis) are correlated by the relationship $uc/a=(3/8)^{1/2}$, where $c/a=(8/3)^{1/2}$ and u=3/8 for an ideal crystal. ZnO crystals deviate from this ideal arrangement by changing both of these values. This deviation occurs such that the tetrahedral distances are kept roughly constant in the lattice. Experimentally, for wurtzite ZnO, the real values of u and c/a were determined in the range u=0.3817–0.3856 and c/a=1.593–1.6035 [93-95]. Additional to the wurtzite phase, ZnO is also known to crystallize in the cubic zincblende and rocksalt (NaCl) structures, which are illustrated in figure 2.1(b) and (c). Zincblende ZnO is stable only by growth on cubic structures [96-98], whilst the rocksalt structure is a high-pressure metastable phase forming at ~10 GPa, and cannot be epitaxially stabilized [99]. Theoretical calculations indicate that a fourth phase, cubic cesium chloride, may be possible at extremely high temperatures, however, this phase has yet to be experimentally observed [100].

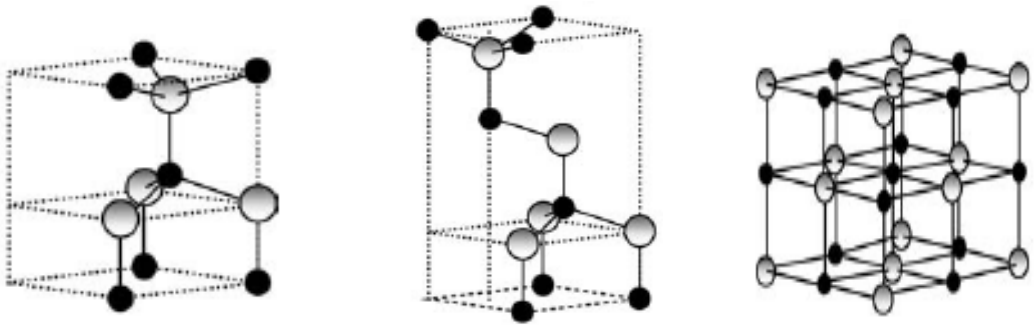

(a) (b) (c)

Figure 2.1: The hexagonal wurtzite (B4) (a), zincblende (B3) (b) and rocksalt (B1) (c) phases of ZnO. Zn atoms are shown as gray spheres, O atoms as black spheres. Only one unit cell is illustrated for clarity. Hadis Morkoc et al. [124].

2.2.2. Energy band structures

ZnO semiconductors are suitable candidate to discover applications for gas sensors, magnetic devices, fabrication of excitonic optical devices and transistors. The basic parameters of the crystal structures and physical properties of ZnO are shown in Table 2.1. ZnO is a direct bandgap semiconductor with the band edge at the Γ-point is triply degenerate. Table 2.2 shows the atmospheric pressure bandgap, the pressure dependence of the bandgap, the exciton binding energy, and exciton energy levels at 6K [11,91].

Table 2.1: Crystal structures and fundamental parameters of electronic properties of ZnO. [1]

Materials	ZnO
bandgap energy (RT) (eV)	3.37
exciton binding energy (meV)	59–63
biexciton binding energy (meV)	15
effective electron mass	0.24–0.28m_0
effective hole energy mass (HH)	1.8m_0
crystal structure	hexagonal
lattice constant (˚A)	a = 3.250, c = 5.207
bond length (˚A)	1.99

Table 2.2: Band parameters of ZnO at 6K. [1]

Valence Band	Atmospheric Pressure Bandgap (eV)	Pressure Dependence of Bandgap (dEg/dP) (meV G/Pa)	exciton Binding Energy (meV)	Exciton Energy Level (eV)
A	3.4410	24.7	63.1	3.37785 (1s), 3.4252 (2p)
B	3.4434	25.3	50.4	3.39296 (1s), 3.4308 (2p)
C	3.4817	26.8	48.9	3.4327 (1s), 3.4694 (2p)

The electronic band structure of ZnO has been calculated by a number of groups [102-108]. The results of a band structure calculation using the Local DensityApproximation (LDA) and incorporating atomic self-interaction corrected pseudopotentials (SIC-PP) to accurately account for the Zn 3*d* electrons is shown in figure 2.2 [109]. The band structure is shown along high symmetry lines in the hexagonal Brillouin zone. Both the valence band maxima and the lowest conduction band minima occur at the Γ point k=0 indicating that ZnO is a direct band gap semiconductor. The bottom 10 bands (occurring around −9 eV) correspond to Zn 3*d* levels. The next 6 bands from −5 eV to 0 eV correspond to O 2*p* bonding states. The first two conduction band states are strongly Zn localized and correspond to empty Zn 3*s* levels. The higher conduction bands (not illustrated here) are free-electron-like. The O 2*s*

bands (also not illustrated here) associated with core-like energy states, occur around −20 eV. The band gap as determined from this calculation is 3.77 eV. This correlates reasonably well with the experimental value of 3.4 eV, and is much closer than the value obtained from standard LDA calculations, which tend to underestimate the band gap by ~3 eV due to its failure in accurately modeling the Zn 3*d* electrons. In addition to calculations for the band structure of bulk ZnO, Ivanov and Pollmann[106] have also carried out an extensive study on the electronic structure of the surfaces of wurtzite ZnO. Using the empirical tight-binding method (ETBM) to determine a Hamiltonian for the bulk states, the scattering theoretical method was applied to determine the nature of the surface states. The calculated data was found to be in very good agreement with experimental data obtained from electron-energy-loss spectroscopy (EELS) and ultra-violet photoelectron spectroscopy (UPS).

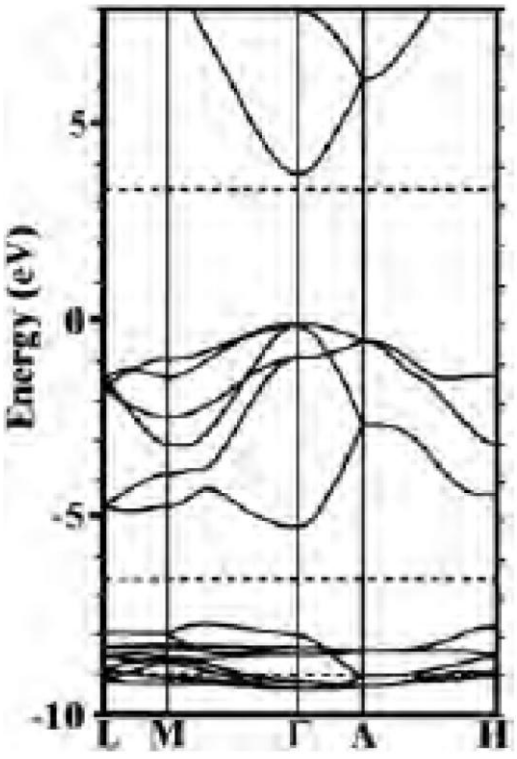

Figure 2.2: The LDA band structure of bulk wurtzite ZnO calculated using dominant atomic self-interaction-corrected pseudopotentials (SIC-PP). This method is much more efficient at treating the d-bands than the standard LDA method [108,125].

Figure 2.3 shows the wave-vector-resolved local density of states (LDOSs) on the first three layers of the (0001)-Zn (left panel) and $(000\bar{1})$-O (right panel) surfaces, for the Γ, M and K points of the surface Brillouin zone. The bulk LDOS (calculated using the ETBM) is given by the dashed lines. Surface induced positive changes to the LDOS are shown as hatched. The properties of the two polar faces are expected to be different, and this is reflected in this data. Whilst it indicates that no surface states are present in the band gap, the Zn surface shows an increase in back bonds (denoted by B in figure 2.3) and anti-back bonds (denoted by A) surface states, while the O face simply shows an increase in P resonances and states. This result suggests that the Zn face possesses more covalent character, arising from the Zn 4*s*–O 2*p* states, whilst the O face is more ionic.

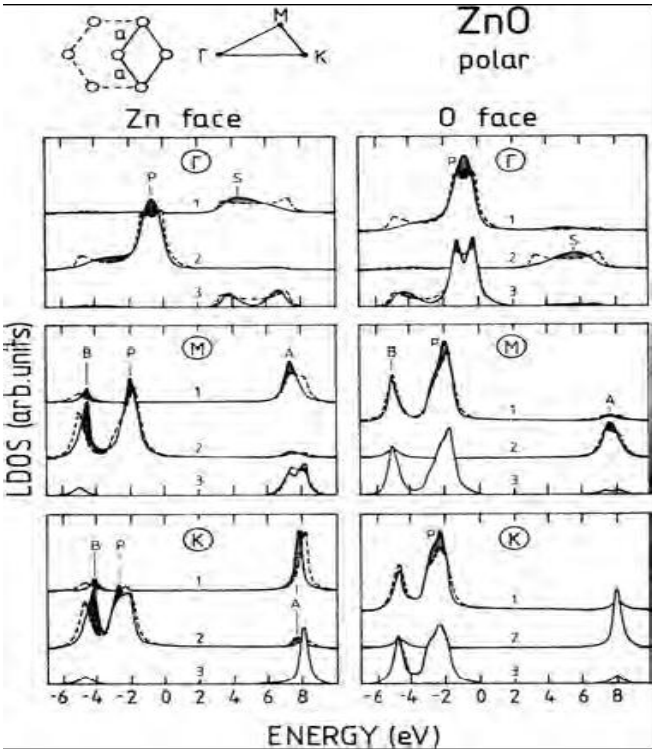

Figure 2.3: Wave-vector-resolved LDOS's on the first three layers of the (*0001*)-Zn (left panel) and (*0001*)-O (right panel) surfaces. The bulk LDOS is given by the dashed lines and surface induced positive changes to the LDOS are shown as hatched. The letters A, B, P and S represent anti-back bonds, back bonds, P resonances and S resonances respectively. [108,125].

2.2.3. Mechanical properties

Table 2.3 gives a brief overview of the well accepted and experimentally useful parameters describing the mechanical properties of ZnO. As seen from the table, ZnO is a relatively soft material, with a hardness of ~5 GPa at a plastic penetration depth of 300 nm (for *c*-axis oriented bulk ZnO) [126]. This needs to be taken into consideration when processing and designing ZnO-based devices. Nanoindentation studies conducted by Bradby et al. [127] of ZnO with a spherical indenter of radius ~4.2μm have shown that the primary mechanism for deformation in this semiconductor is the nucleation of slip on the basal and pyramidal planes. For loads of up to 50 mN, there has been no observation of phase transformations or cracking in this material. Nanoindentation is a useful technique for probing the mechanical properties of a material, whilst also providing information on the behavior of a material under contact induced damage, such as that experienced during device processing. For ZnO, indentation results in significant quenching of the excitonic luminescence. Additionally, extensive damage is created in the ZnO material, with defects propagating far beyond the volume under contact [127].

Table 2.3: Key mechanical properties of *c*-axis oriented wurtzite ZnO, as determined by experiment and theory [125].

Parameter	**Experimental**	**Theoretical**
Bulk Young's modulus, E (GPa)	111.2 ± 4.7	
Bulk hardness, H (GPa)	5.0 ± 0.1	
Epitaxial Young's modulus, E (GPa)	310 ± 40	
Epitaxial hardness, H (GPa)	5.75 ± 0.8	
Bulk modulus, B (GPa)	142.4	156.8
dB/dP	3.6	3.6
e_{33} ($C\ m^{-2}$)	0.96	1.19

e_{31} *(C* m^{-2}*)*	−0.62	−0.55
e_{15} *(C* m^{-2}*)*	−0.37	−0.46
Spontaneous polarization (C m^{-2})		−0.047
c_{11} *(GPa)*	209	246
c_{33} *(GPa)*	216	246
c_{12} *(GPa)*	120	127
c_{13} *(GPa)*	104	105
c_{44} *(GPa)*	44[h]	56[f]
Born effective charge, Z*		2.1[g]

2.2.4. Optical properties

The optical properties of ZnO are heavily influenced by the energy band structure and lattice dynamics. For a comprehensive review of the optical properties of excitonic recombinations in bulk, *n*-type ZnO, B. K. Meyer et al.[110] gives a comprehensive treatment and analysis of the excitonic spectra obtained from ZnO, and assigns many defect related spectral features, as well as donor–acceptor pair (DAP) emission. A broad defect related peak extending from~1.9 to~2.8 eV is also a common optical feature of ZnO. Known as the green band, the origin of its luminescence is still not well understood and has in the past been attributed to a variety of different impurities and defects. Figure 2.4 shows a typical photoluminescence spectra of *n*-type ZnO measured at 4.2 K. The excitonic, DAP and extended green band emission can all be clearly seen, as can the phonon replicas produced from the longitudinal optical phonons (LO). Due to the lack of available data on *p*-type ZnO, a corresponding spectrum is not shown here. In terms of the more fundamental optical properties of ZnO, there have been a number of comprehensive studies to determine the refractive index and dielectric constants of this material [111-113]. The measurements were

all carried out using spectroscopic ellipsometry. The values determined for the dielectric constants of ZnO are shown in table 2.4 whilst the refractive index dispersion for both $E \perp c$ and $E \| c$ as measured and calculated by Yoshikawa and Adachi [111] is shown in figure 2.5.

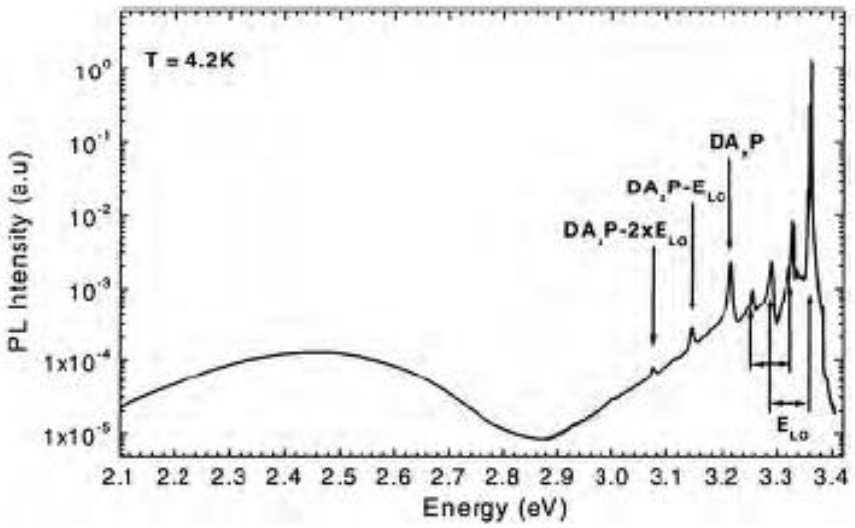

Figure 2.4: Photoluminescence spectrum of *n*-type bulk ZnO (HeCd excitation) showing excitonic, donor acceptor pair and green-band emission. The longitudinal optical phonons with the corresponding phonon replicas are indicated on the figure [110].

Table 2.4: Static (ε_o) and high frequency dielectric constant (ε_∞) data for ZnO [111-112].

		Film [122]	**Bulk [122]**	**Bulk [121]**
ε_o	$E \perp c$	7.46	7.77	
	$E \| c$	8.59	8.91	
ε_∞	$E \perp c$	3.7	3.6	3.68
	$E \| c$	3.78	3.66	3.72

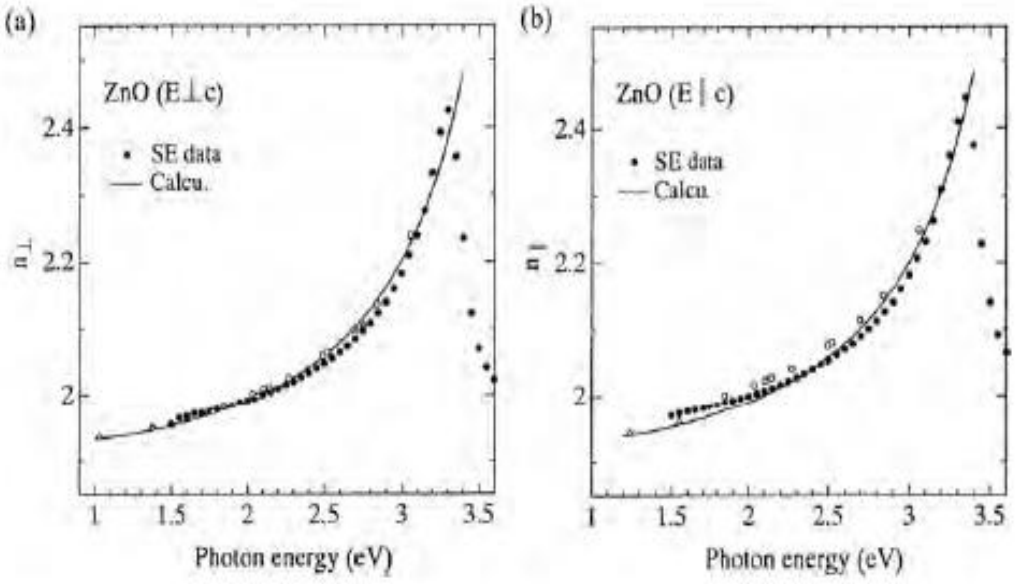

Figure 2.5: Refractive index dispersion of ZnO for E $\perp$ *c* and E $\|$ c below the fundamental absorption edge. The solid circles represent the spectroscopic ellipsometry data whilst the solid line is calculated data. [111]

2.2.5. Electrical properties

The electrical properties of ZnO have been difficult to quantify due to large variance of the quality of samples available. The background carrier concentration varies a lot according to the quality of the layers but is usually$\sim 10^{16}$ -10^{17}cm^{-3}. Hall effect is the most widely used technique to measure the transport properties and assess the quality of epitaxial layers. For semiconductor materials, it yields the carrier concentration, its type, and carrier mobility. More specifically, experimental data on Hall measurements over a wide temperature range (4.2–300 K) provide quantitative information on impurities, imperfections, uniformity, scattering mechanisms, and so on. The Hall coefficient and resistivity (r) are experimentally determined and then related to the electrical parameters through (for n-type conduction) $R_H=r_H/ne$ and $\mu_H=R_H/\rho$, where n is the free electron concentration, e is the unit electronic charge, μ_H is the Hall mobility, and r_H is the Hall scattering factor that depends on the particular scattering mechanism. The drift mobility is the average velocity per unit electric

field in the limit of zero electric field and is related to the Hall mobility The largest reported *n*-type doping is $\sim 10^{20}$ electrons cm^{-3} and largest reported *p*-type doping is $\sim 10^{19}$ holes cm^{-3}, however such high levels of *p*-conductivity are questionable and have not been experimentally verified [125]. Table 2.5 gives the selected best values of electron mobility and corresponding carrier concentration in bulk and thin-film ZnO grown by various techniques.

Table 2.5: Compilation of XRD results, electron mobilities, and corresponding carrier concentrations obtained in nominally undoped bulk and thin-film ZnO deposited on different substrates by various growth techniques. [124]

Sample	**FWHM of XRD rocking curves (arcsec)**	**Carrier concentration (cm^{-3})**	**Electron mobility ($cm^2 V^{-1} s^{-1}$)**	**References**
ZnO thin films grown on MgZnO buffered ScAlMgO4 substrates by PLD	<12(0002) <12($10\bar{1}1$)	1×10^{16}	440	[138]
Bulk ZnO grown by pressurized melt method	49 (0002)	5.05×10^{17}(296 K) 3.64×10^{16}(77K)	131(296 K) 298(77K)	[139]
ZnO thin films grown on c-plane sapphire substrates by PLD	18(0002) 151(0002)	8×10^{13}(Li compensated) 2.0×10^{16}	200 155	[140] [139]

ZnO thin films grown on *c*-plane sapphire with ZnO/MgO	18 (0002) 1076 (1011)	1.2×10^{17}	130	[141]

2.3. ZnO Growth

Growth of zinc oxide (ZnO) thin films has been propelled by a variety of methods, operated by applications such as acoustical and optical devices. The applications have been driven in part due to the outstanding piezoelectric characteristics of ZnO and its affinity to grow with strong (0 0 0 1) preferential orientation on various kinds of substrates, including glass [111], sapphire [112], and diamond [132]. The early reports dealt with deposition of ZnO utilizing growth techniques such as magnetron sputtering [73] and chemical vapor deposition [72]. However, the films were mainly polycrystalline. Later approach paved the way to high-quality ZnO single-crystal films prepared by radio frequency (RF) magnetron sputtering [110,133] and other growth techniques that allow fine control over the deposition procedure. Among the latter deposition techniques are molecular beam epitaxy (MBE) [68,111], pulsed laser deposition (PLD) [73,134], organometallic vapor-phase epitaxy (OMVPE) [6], and hydride or halide vapor-phase epitaxy (HVPE), depending on the chemistry used [135, 136].

2.3.1. Epitaxial Growth Techniques

Device applications in several cases necessitate growth of thin films and multilayers. General epitaxial deposition methods used for semiconductors are applied to ZnO as well. Among these methods, RF sputtering and pulsed laser deposition generally have limitations

as they can provide material with up to certain quality, and mode-advanced techniques such as molecular beam epitaxy and chemical vapor deposition are required to improve the thin film crystallinity further. In terms of substrates, other than bulk ZnO for homoepitaxial growth, ZnO and associated materials have been grown on foreign substrates, most common ones being sapphire and GaN. In this section, deposition of ZnO will only focus on the RF magnetron sputtering since our work is based on this deposition technique.

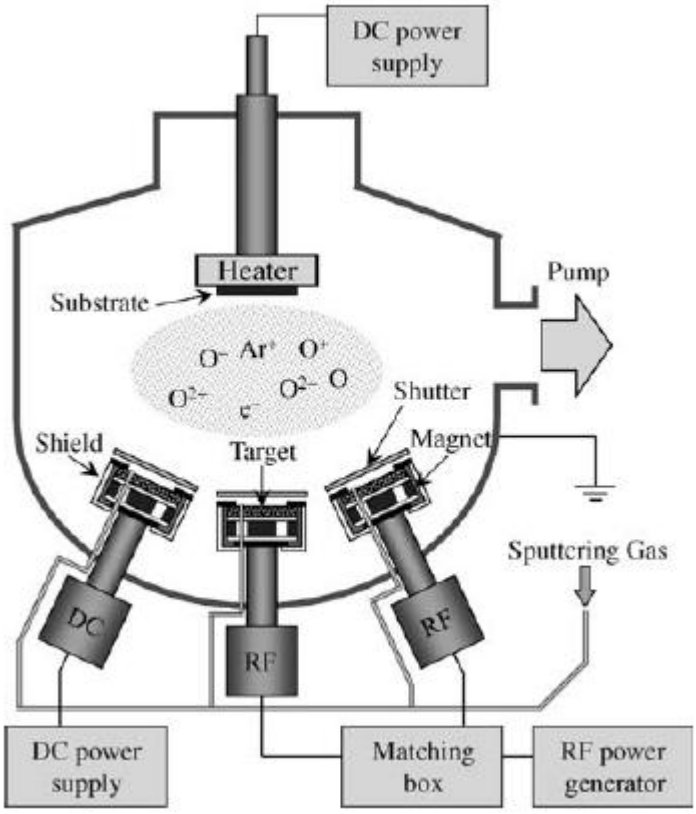

Figure 2.6: Schematic diagram illustrating an RF magnetron sputtering system combined with a DC power supply for applying a bias voltage to the substrate.

2.3.2. RF Magnetron Sputtering

One of the most popular growth techniques during the early ZnO investigations was sputtering (DC sputtering, RF magnetron sputtering, and reactive sputtering). As compared to sol–gel (spin-on method) and chemical vapor deposition [69], the magnetron sputtering

was a preferred method because of its low cost, simplicity, and low operating temperature, as well as the reasonable quality of the resultant films [137-138]. The schematic diagram of a typical RF magnetron sputtering system is shown in Figure 2.6. In magnetron sputtering, the growth is usually carried out in an ambient of $O_2/Ar+O_2$ with ratios ranging from 0 to 1 at a pressure of 10^{-3}–10^{-2} Torr. O_2 serves as the reactive gas and Ar acts as the sputtering enhancement gas. ZnO can also be grown by DC sputtering from a Zn target in an $Ar+O_2$ gas mixture. The RF power applied to the plasma is tuned to regulate the sputtering yield rate from the ZnO target. For these experiments, the target is pre-sputtered for 5-15 min before the actual deposition begins to remove any contamination on the target surface, make the system stable, and reach optimum conditions.

2.4. Wide Band Gap Semiconductor Ultraviolet Photodetectors

Ultraviolet (UV) radiation was first mentioned in 1801, when J W Richter discovered that certain chemical reaction were catalyzed by exposure to non-visible radiation with a shorter wavelength than violet. Soon after this discovery, in 1804, T. Young confirmed that this chemically active radiation followed the interference laws. This observation, significantly together with the work of many other researchers, made it possible to establish that both visible and UV emissions were manifestations of the same kind of electromagnetic radiation, only differing in their wavelength. [123]

Nowadays, it is widely accepted that the UV region occupies the spectral interval of λ = 400–10 nm. It is a highly ionising energy, which activates many chemical processes. The most important natural UV source is the Sun. Approximately 9% of the energy received from the Sun at the higher layers of the atmosphere is in the UV range, although the stratospheric ozone layer prevents wavelengths shorter than 280 nm from reaching the Earth's surface. As well, remaining UV radiation may be attenuated by pollution in the low troposphere. [123]

UV radiation is commonly divided into three regions; as function of its effects in the biosphere:

UV A (400-320 nm). This is the less energetic range. It stimulates photosynthesis, and is involved in the synthesis of some vitamins and basic biochemical compounds. Overexposure may lead to erythema and premature ageing. New research has been found that it is also causing skin cancer. [123]

UV-B (320–280 nm). Even though partially absorbed by the ozone layer, this composes 10% of the total UV radiation reaching the Earth's surface. UV-B exposure is harmful for human beings (causing skin cancer, cataracts, burns, erythema), negatively affects harvests and enhances the ageing of organic materials. It also presents some beneficial properties, such as the activation of D vitamin. [123]

UV-C (280–10 nm). UV-C rays are the highest energy, most dangerous type of ultraviolet light. However, it is almost completely absorbed by the stratospheric ozone layer. Little attention has been given to UVC rays in the past since they are filtered out by the atmosphere. However, their use in equipment such as pond sterilization units may pose an exposure risk, if the lamp is switched on outside of its enclosed pond sterilization unit.

A further widespread division of the UV region is as follows: near-UV, 400–300 nm; middle-UV, 300–200 nm; far-UV, 200–100 nm; extreme-UV, 100–10 nm. For chronological reasons, it is also common to speak about vacuum ultraviolet (VUV), which corresponds to the spectral range that is absorbed by oxygen (200–10 nm), thus requiring experimentation in vacuum. The detection of UV radiation offer a wide range of civil and military applications, such as chemical and biological analysis (ozone, pollutants, and most organic compounds present absorption lines in the UV spectral range), astronomical studies, optical communications (particularly inter-satellite communications at $\lambda < 280$ nm), emitter calibration (instrumentation, UV lithography), and flame detection (including fire alarms, missile warning or combustion monitoring). [123]

2.5. Photodetector parameters

Among photoelectric detectors, we can distinguish semiconductor detectors and photoemissive detectors (photocathodes). In a photo-emissive detector, when photons impact the photosensing material in the cathode, electrons are emitted into vacuum. The voltage difference applied between the photocathode surface and the anode make it possible to collect the electrons and measure the ensuing current. On the contrary, in semiconductor photodetectors, photons are absorbed in the semiconductor, creating electron–hole pairs. These photogenerated carriers are separated by the electric field, due either to the built-in potential or the applied voltage, producing a current proportional to the photon flux. There are different types of semiconductor photodetectors: photoconductors, Schottky barrier photodiodes, metal–semiconductor–metal (MSM) photodiodes, metal– insulator–semiconductor (MIS) structures, p–n and p–i–n photodiodes, and field-effect and bipolar phototransistors. [123]

The important parameters of semiconductor photodetectors are the following:

1. Responsivity

The responsivity of a photodetector is the ratio of its output electrical signal, either a current I_{out} or voltage V_{out} to the input optical signal expressed in terms of the incident optical power P_{op}**.** One can define a current responsivity and a voltage responsivity using respectively:

$$R_i = \frac{I_{out}}{P_{op}} \text{ and } R_v = \frac{V_{out}}{P_{op}} \quad (2.1)$$

Responsivity is also determined by the quantum efficiency (number of electron–hole pairs generated per incident photon) and gain (number of carriers detected per photogenerated electron–hole pair), responsivity (*Ri*), gain (*g*) and quantum efficiency (η), using the following expression:

$$R_i = \frac{\lambda \eta}{hc} qg \quad (2.2)$$